

## Quantum chromodynamics: calculations

Calculations in QCD have been made in two ways: lattice simulations at low energies, and perturbative calculations at high energies. In this chapter we outline some of the results obtained.

### 17.1 Lattice QCD and confinement

It was pointed out in Section 16.1 that, at low energies, a non-perturbative approach to QCD is needed. ‘Lattice QCD’ is such an approach. The gluon fields are defined on a four-dimensional lattice of points  $(n^\mu, \mathbf{n})a$ , where  $a$  is the lattice spacing and the  $n^\mu$  are integers. Field derivatives are replaced by discrete differences. This gives a ‘lattice regularised’ QCD. The lattice spacing corresponds to an ultraviolet cut-off, since wavelengths  $< 2a$  cannot be described on the lattice. A lattice does not have full rotational symmetry in space, but it is believed that nevertheless continuum QCD corresponds to the limit  $a \rightarrow 0$ . Current computing power allows lattices of  $\sim(36)^4$  points. The range of the strong nuclear force is  $\sim 1$  fm. To fit such a distance comfortably on the lattice, we can anticipate that we shall not want  $a$  to be much less than  $(2\text{fm})/36 = 0.056\text{fm}$  (and  $\hbar c/a > 3.5$  GeV).

In the high energy perturbation theory described in Section 16.3, the renormalisation parameter  $\lambda$  and the dimensionless coupling parameter  $g$  are combined to give a single physical parameter,  $\Lambda$ , having the dimensions of energy. The relationship between the effective coupling constant  $\alpha_s(Q^2)$  and  $\Lambda$  in the lowest order of perturbation theory is given by (16.25). In lattice QCD, the unphysical lattice parameter  $a$  and the dimensionless coupling parameter  $g(a)$  combine to give a single physical parameter  $\Lambda_{\text{latt}}$ , having the dimensions of energy. In the lowest order

of ‘lattice’ perturbation theory, as  $a \rightarrow 0$  then  $g(a) \rightarrow 0$ ,

$$g^2(a) = \frac{-16\pi^2}{11 \ln(a^2 \Lambda_{\text{latt}}^2)} \quad (17.1)$$

(see Hasenfratz and Hasenfratz, 1985).

$\Lambda_{\text{latt}}$  is independent of  $a$  in the limit  $a \rightarrow 0$ . This remarkable feature of the theory is called *dimensional transmutation*.

Equation (17.1) may be compared with (16.25) with  $n_f$  set equal to zero. It can be shown theoretically (Dashen and Gross, 1981) that

$$\frac{\Lambda_{\text{latt}}}{\Lambda} = \text{constant} \approx \frac{1}{30}. \quad (17.2)$$

The precise value of the constant depends on the renormalisation scheme in which  $\Lambda$  is defined, and the number of quark flavours included.  $\Lambda_{\text{latt}}$ , or equivalently  $\Lambda$ , is to be determined from experiment. We shall see in Section 17.3 that  $\Lambda$  is known to be  $\sim 300$  MeV, so that  $\Lambda_{\text{latt}} \sim 10$  MeV. We can then infer from equation (17.1) that for  $a \sim 0.056$  fm, the coupling constant  $g$  should be of order 1.

Lattice QCD calculations have been made to compute the potential energy of a fixed quark and an antiquark in a colour singlet state, as a function of their separation distance. The form of this potential at short distances was discussed in Section 16.4. Non-perturbative lattice calculations have been made in the quenched approximation, excluding effects of virtual quark pair creation.

In the lattice calculations, distances are measured in units of  $a$ , and energies in units of  $(1/a)$ . A coupling constant  $g$  is chosen, and the quark and antiquark are localised on lattice sites that are spatially fixed at a distance apart of  $r = |\mathbf{n}|a$ , where  $\mathbf{n}$  is a set of three integers. The field energy  $E(r)$  generated by the quark–antiquark pair is computed for a sequence of separation distances, and is found to be of the form

$$E(r) = 2A + Kr - \frac{4}{3} \frac{\alpha_{\text{latt}}(r)}{r}, \quad (17.3)$$

where  $A$  and  $K$  are constants, and the factor  $(4/3)$  has been inserted to facilitate comparison with the perturbation results of Section 16.4. The constant  $2A$  can be interpreted as a contribution to the rest energies of the quark and antiquark, and is absorbed into their notional masses to leave an effective potential energy

$$V(r) = Kr - \frac{4}{3} \frac{\alpha_{\text{latt}}(r)}{r}. \quad (17.4)$$

The results of such a calculation by Bali and Schilling (1993) using a  $(32)^4$  lattice are shown in Fig. 17.1. In this calculation  $g = 0.97$ . The term  $Kr$  dominates at large distances. The constant  $K$  is called the *string tension*. In quenched QCD on a lattice, with  $g$  fixed, there is only one energy parameter  $a^{-1}$  (or  $\Lambda_{\text{latt}}$ ). Hence

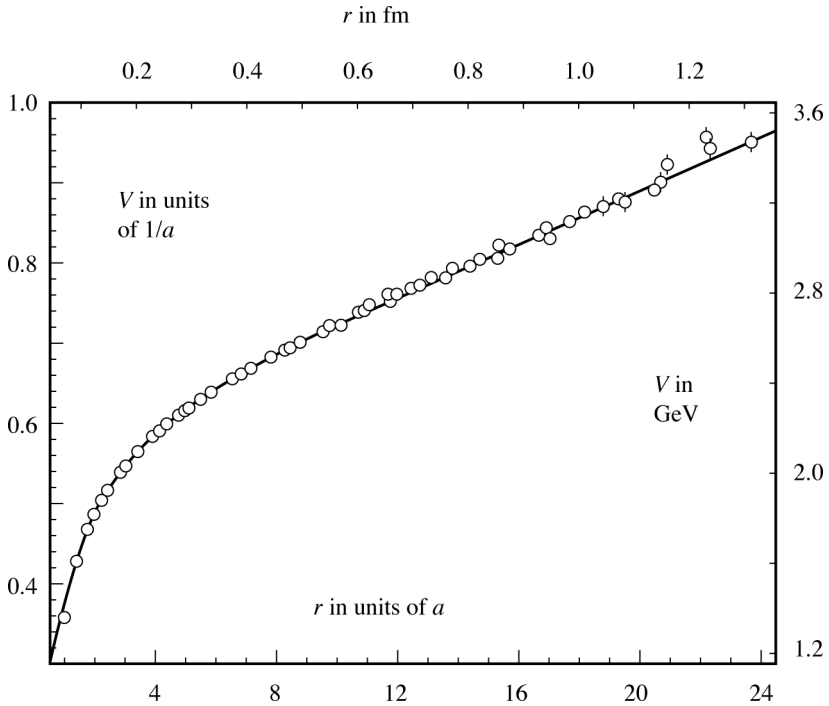


Figure 17.1 The colour singlet quark–antiquark potential as computed on a lattice. For a fixed value of the coupling constant  $g$  (of order 1)  $V(r)$  is computed in lattice units ( $r$  in units of  $a$ ,  $V$  in units of  $1/a$ ). The computed points are fitted with a curve of the form

$$V(r) = 2A + Kr - (c/r) + (f/r^2).$$

In this example  $g$  was fixed at 0.97. The calculation determined  $K = 0.0148$ ;  $K$  is the string tension in units of  $1/a^2$ . The phenomenology of  $c\bar{c}$  and  $b\bar{b}$  quark systems suggests  $K \approx (440 \text{ MeV})^2$ . Taking this value determines  $a = 0.055 \text{ fm}$  and  $1/a = 3.58 \text{ GeV}$ . It also determines one point on the curve  $g(a)$  as a function of  $a$ . The calculations must be repeated to compute  $a$  for several values of  $g$  to check the extent to which the asymptotic form, like equation (17.1), is obeyed ( $\Lambda_{\text{latt}}$  is independent of  $a$ ) in order to be confident of the continuum limit (Bali and Schilling, 1993).

$K$  has the dimensions of  $a^{-2}$ . Bali and Schilling (1993) find  $K = 0.01475(29)a^{-2}$ . In Chapter 1, Fig. (1.5) shows the experimental spectra of the heavy quark systems charmonium ( $c, \bar{c}$ ) and bottomonium ( $b, \bar{b}$ ). Many fits to these spectra have been made using a Schrödinger equation with an interaction potential of the form (17.3). In the lowest energy states of heavy quark systems, the quark and antiquark are slowly moving, so that a non-relativistic approximation is reasonable. The spectra are well fitted with  $K = (440 \text{ MeV})^2 = 1 \text{ GeV fm}^{-1}$ ,  $\alpha(r) = \text{constant} = 0.39$ .

Taking  $K = (440 \text{ MeV})^2$  fixes the lattice spacing  $a = 0.0544 \text{ fm}$ , and  $a^{-1} = 3.62 \text{ GeV}$ .

Equation (17.1) could now be used to estimate  $\Lambda_{\text{latt}}$ . However, this equation (and more sophisticated extensions to higher orders of lattice perturbation theory) hold only in the limit  $a \rightarrow 0$ . To extract  $\Lambda_{\text{latt}}$  reliably, the calculations must be repeated for different values of  $g$ . The corresponding values of  $a$  follow from the string tension. The limit  $\Lambda_{\text{latt}}$  as  $a \rightarrow 0$  may then be estimated. Bali and Schilling (1993) found  $\sqrt{K}/\Lambda_{\text{latt}} = 51.9_{-1.8}^{+1.6}$ , which is consistent with the value  $\sqrt{K}/\Lambda_{\text{latt}} = 49.6$  (3.8) estimated by Booth *et al.* (1992) from results on a  $(36)^4$  lattice. Taking  $\sqrt{K} = 440 \text{ MeV}$  gives  $\Lambda_{\text{latt}} \approx 8.5 \text{ MeV}$ , and from (17.2)  $\Lambda \approx 255 \text{ MeV}$ .

At small  $r$  the attractive Coulomb-like term dominates. It is found that  $\alpha_{\text{latt}}(r)$  is a slowly varying function of  $r$  that decreases with decreasing  $r$ , as expected from perturbation theory (Section 16.3). The potential of Fig. 17.1 is well fitted with

$$\alpha_{\text{latt}}(r) = 0.236 - (0.0031 \text{ fm})/r.$$

This is to be compared with the value of  $\alpha = e^2/4\pi \approx 1/137$  of QED.

It is interesting to note that the linearly rising term in the potential is computed in the quenched approximation. If quantum fluctuating quark fields were to be included, the large potential energy available at large separation distances of the fixed quark and antiquark pair would produce pairs of quarks and antiquarks. A quark would migrate to the neighbourhood of the fixed antiquark to form a colour singlet, and an antiquark would similarly form another singlet with the fixed quark, resulting in two well separated mesons.

## 17.2 Lattice QCD and hadrons

Systems of quarks and antiquarks held together by the associated gluon field are called *hadrons* (see Section 1.4). For example, the proton, the only stable hadron, has up quark number two and down quark number one. Other systems, for example mesons, are held together only transiently by their gluon field. As well as these so-called *valence quarks* that define a system, a hadron contains quark–antiquark pairs excited by the gluon field, and known as *sea quarks*.

So far, in our discussion of hadrons and confinement, sea quarks have been neglected. Convincing calculations of hadron properties require their inclusion especially  $u\bar{u}$ ,  $d\bar{d}$  and  $s\bar{s}$  pairs which because of their small masses with respect to  $\Lambda_{\text{QCD}}$  are readily excited by the gluon field. Since the first edition of this book, much progress in lattice QCD has been made to include these pairs.

Quarks on the lattice require the introduction of quark masses. In the work of Davies *et al.* (2004) calculations are made with  $m_u = m_d$  (the isospin symmetry limit: see Section 16.6). A mean mass  $(m_u + m_d)/2$  is introduced along with the masses  $m_s, m_c, m_b$ , and the strong coupling constant  $g$ : five parameters in all. With a fixed value of  $g$  the lattice spacing  $a$  and the four quark masses are determined by fitting the five experimentally determined masses  $m(b\bar{b}1s) = 9.460 \text{ GeV}$ ,  $m(b\bar{b}2s) = 10.023 \text{ GeV}$  (see Figure 1.5),  $m_\pi = 0.139 \text{ GeV}$ ,  $m_K = 0.496 \text{ GeV}$  and  $m_D = 1.867 \text{ GeV}$ . The  $D^+$  meson  $D(c\bar{s})$  is the ground state of the  $c\bar{s}$  valence quark system.

As in Section 17.1 the lattice spacing  $a$  is a function of  $g$  and so also are the quark masses. The calculations have to be repeated for different values of  $g$  to extract  $\Lambda_{\text{latt}}$  and  $g(a)$  and the four quark masses which are also taken to be functions of  $a$ . They can also be regarded as function of energy,  $\hbar c/a$ . The fact that the strong coupling constant and quark masses are functions of the energy at which they are measured is a natural feature of QCD. The calculations give, at an energy of 2 GeV for the light quarks

$$\begin{aligned} \left(\frac{m_u + m_d}{2}\right) (2 \text{ GeV}) &= 3.2 \pm 0.4 \text{ MeV} \\ m_s (2 \text{ GeV}) &= 87 \pm 8 \text{ MeV} \\ m_c &= 1.1 \pm 0.1 \text{ GeV} \\ m_b &= 4.25 \pm 0.15 \text{ GeV} \\ \alpha_s (M_Z) &= 0.121 \pm 0.003. \end{aligned}$$

and

$m_c$  and  $m_b$  are quoted at their own mass scale and it is conventional to quote  $\alpha_s$  at the scale of the Z boson. To find the parameters at different scales their energy dependence is given by equations like (16.25).

Having values for the parameters of QCD its validity can be tested by confronting independent experimental data with calculations. At present one is confined to single hadrons that are stable to the strong interaction. Unstable particles or those that are close to instability tend to fluctuate outside the lattice boundaries. Also the baryons, and in particular the proton and neutron that carry u and d valence quarks can not yet be reliably handled on the lattice. Nevertheless many particle properties lend themselves to lattice calculations and the success in fitting data is impressive. Figure 17.2 shows results taken from Davies *et al.* (2004). Ten calculations are compared with experiment. The results are expressed as the calculated divided by the experimental value. The experimental values are accurately known and the errors that bracket the mean values indicate the estimated accuracy of the calculation. It seems that with present computing power, theory and experiment agree to better

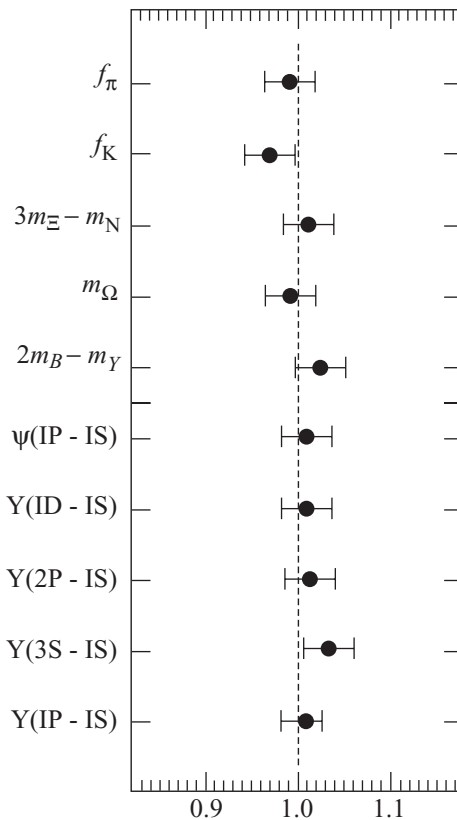


Figure 17.2 Quantities calculated in lattice QCD divided by their experimental values:

$$f_\pi = \alpha_\pi / \sqrt{2} G_F V_{ud} \quad \text{see Section 9.2,}$$

$$f_K = \alpha_K / \sqrt{2} G_F V_{us} \quad \text{see Problem 9.10.}$$

$m_\Omega$  is the mass of the  $\Omega(sss)$ , the ground state of the baryon with s quark number three.

$3m_\Xi - m_N$  is a combination of ground state baryon masses  $\Xi(ssu)$  and the neutron  $N(ddd)$ .

The other mass differences are between states of the  $c\bar{c}$  and  $b\bar{b}$  mesons (Davies *et al.*, 2004).

than 4%. There is no reason here to doubt the validity of QCD as the theory of strong interactions.

### 17.3 Perturbative QCD and deep inelastic scattering

One of the first applications of perturbative QCD was to the  $Q^2$  dependence of the parton distribution functions of the proton. In the parton model of inelastic

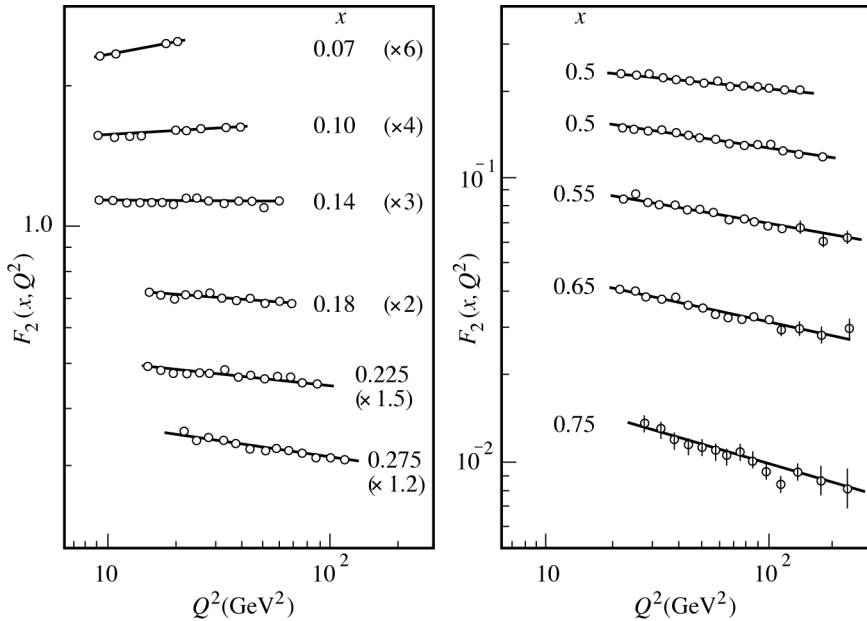


Figure 17.3 The proton structure function  $F_2(x, Q^2)$ . The experimental points are fitted with curves generated by the evolution equations with  $\Lambda = 205 \text{ MeV}$ . To aid reading in the left-hand section, the data have been scaled by the given factors, so for example at  $x = 0.18$  the graph is of  $2F_2(0.18, Q^2)$ . (Taken from *Physics Letters B* **223**, Benvenuti, A. C. *et al.* Test of QCD and a measurement of  $\Lambda$  from scaling violations in the proton structure factor  $F_2(x, Q^2)$  at high  $Q^2$  (Benvenuti *et al.*, p. 490), with kind permission of Elsevier Science-NL, Sara Burgerhartstraat 25, 1005 kv Amsterdam, The Netherlands.)

electron–proton scattering (Appendix D), the proton is described by parton distribution functions  $p_i(x, Q^2)$ , where

$$Q^2 = -q_\mu q^\mu = (\mathbf{p} - \mathbf{p}')^2 - (E - E')^2,$$

$q^\mu = (E - E', \mathbf{p} - \mathbf{p}')$  is the energy and momentum transferred in the inelastic electron scattering, and  $x = Q^2/[2M(E - E')]$  where  $M$  is the proton mass. The partons are identified as quarks, antiquarks and gluons. Typically, at a fixed value of  $Q^2$ , say  $Q_0^2$ , distribution functions  $p_i(x, Q_0^2)$  are extracted from the data, the number of distribution functions being determined by the number of distinct data sets. At this stage the extraction of the distribution functions is merely a matter of curve fitting: although the functions  $p_i(x, Q_0^2)$  should be a consequence of QCD, the problem of establishing their form theoretically is immensely difficult. However, given these distribution functions, and provided  $Q_0^2$  is large enough, perturbative QCD can be used to predict how they evolve with changing  $Q^2$ . This evolution

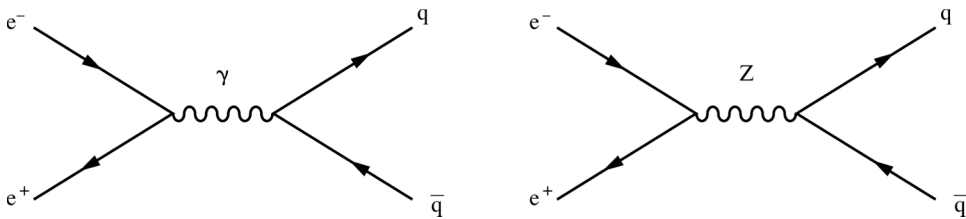


Figure 17.4  $e^+e^-$  annihilation to a quark–antiquark pair with no gluon radiative corrections.

is described by the equations of Altarelli and Parisi (1977), which take account perturbatively of the quark–gluon interactions.

As an example, Fig. 17.3 shows experimental data on the related structure function  $F_2(x, Q^2)$  defined in Appendix D, taken by the BCDMS collaboration (Benvenuti *et al.*, 1989). Also shown are the theoretical predictions, at fixed values of  $x$ , of the QCD evolution as a function of  $Q^2$ . The data are precise and the shapes of all the curves are given by the single parameter  $\Lambda$ . Fits to the data determine  $\Lambda = 205 \pm 80 \text{ MeV}$ , from which one can infer, using (16.25) with  $n_f = 5$ , that  $\alpha_s(M_z^2) = 0.115 \pm 0.007$ .

### 17.4 Perturbative QCD and $e^+e^-$ collider physics

The basic Feynman diagrams for hadron production in  $e^+e^-$  colliding beam experiments are shown in Fig. 17.4. In the range 10 GeV to 40 GeV, electromagnetic processes dominate. The data were discussed in Section 1.7.

Around 90 GeV, close to the centre of mass energy for Z production, the weak interaction dominates. The hadronic decays of the Z were discussed in Chapter 15, using perturbation theory. However, there are additional contributions to the cross-section arising from gluon radiation, for example the processes illustrated in Fig. 17.5.

The modification is simply expressed (see Particle Data Group, 1996). If the hadron production cross-section without gluon radiative corrections is denoted by  $\sigma_0$  then (to order  $\alpha_s^3$ ) the cross-section  $\sigma$  with corrections is

$$\sigma = f\sigma_0,$$

with

$$f = 1 + \frac{\alpha_s}{\pi} + 1.411 \left(\frac{\alpha_s}{\pi}\right)^2 - 12.8 \left(\frac{\alpha_s}{\pi}\right)^3, \quad (17.5)$$

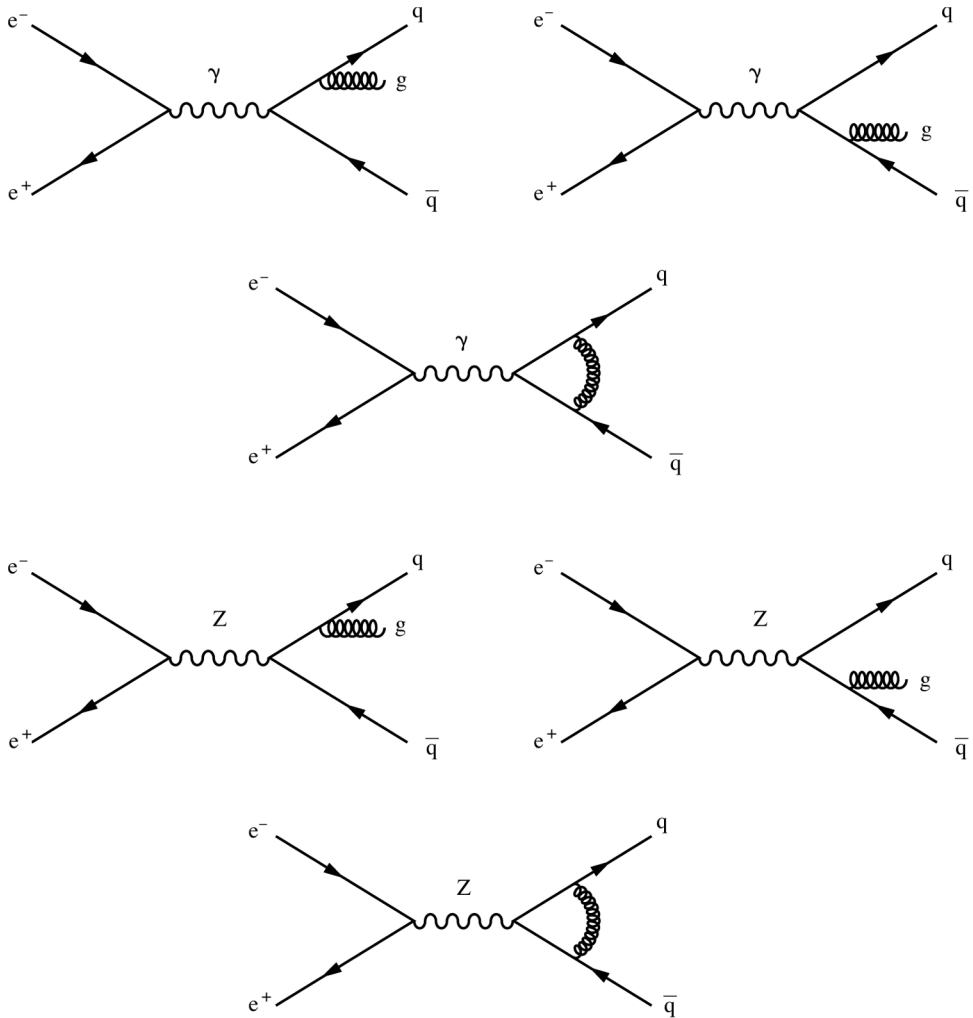


Figure 17.5 The lowest order gluon radiative corrections to quark–antiquark pair production by  $e^+e^-$  annihilation.

and  $\alpha_s(Q^2)$  taken at  $Q^2$  equal to the square of the centre of mass energy. For example, taking  $\alpha_s(M_z^2) = 0.115 \pm 0.007$  from Section 17.3 gives  $f = 1.038 \pm 0.003$ . This is the value of  $f$  used in Chapter 15. Alternatively, the best fit to the hadronic decays of the Z would suggest  $f = 1.041 \pm 0.003$ , which gives  $\alpha_s(M_z^2) = 0.123 \pm 0.007$  and  $\Lambda = 310 \pm 90 \text{ MeV}$ . The consistency of the theory between the two very different experimental regimes: electron–proton scattering and Z decays, from which these estimates are obtained, is impressive.

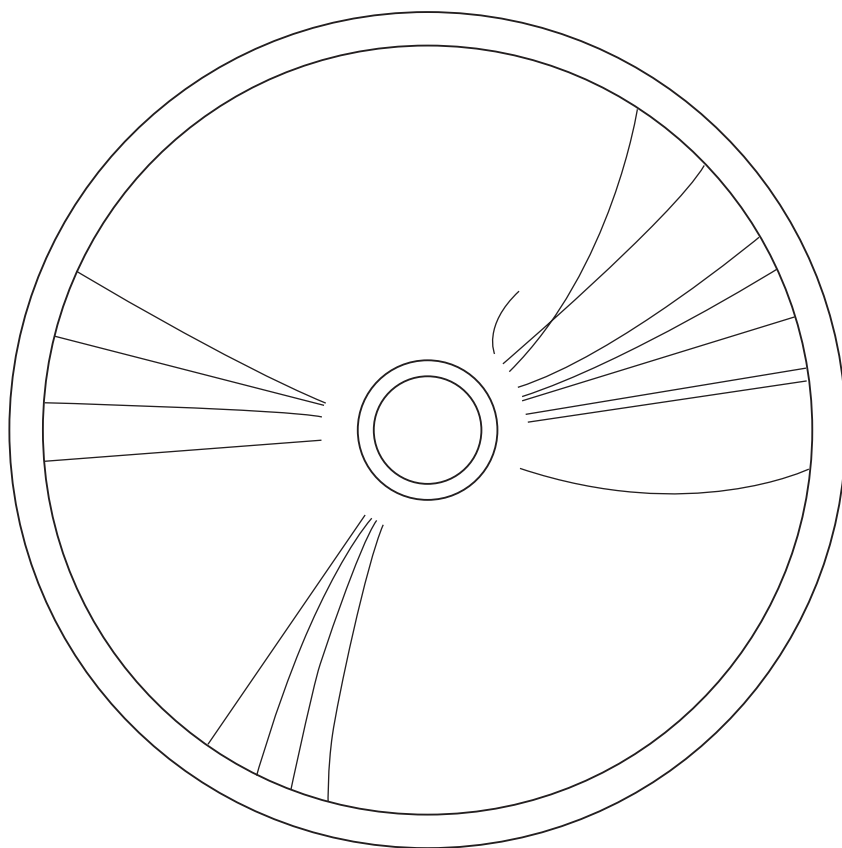


Figure 17.6 A three-jet event recorded by the JADE detector at the PETRA  $e^+e^-$  collider, DESY.

The hadrons produced in most  $e^+e^-$  annihilations at high energies appear in two back to back jets associated with the originating  $q\bar{q}$  pair. Gluon radiation contributing to the  $f$  factor is mostly confined to be within the associated quark or antiquark jet. However, according to perturbative QCD it is also possible for a gluon to be radiated into a distinct region of phase space and appear as a third distinct jet. Figure 17.6 is an example of such a three-jet event. Measurements of these three- and even four-jet events gives further strong support to the theory of QCD.